ARTICLE NO. 78-178R

J80-038

Experimental Investigation of Heat and Mass Diffusion in a Porous Tube-Generated Flowfield

20007
90002

J. M. Avidor* and M. Delichatsios†
Avco Everett Research Laboratory, Inc., Everett, Mass.

Flow of laser gas and a saturable absorber gas generated by two adjacent grids of porous tubes provides a novel scheme for windowless gain isolation of large CO_2 laser amplifiers. Turbulent mixing at the interface of the two parallel flows causes laser beam degradation, and a reduction in the available active laser volume due to mass diffusion. In the present study, hot wire anemometry, species concentration measurements, and interferometry were used to investigate and to visualize the turbulent diffusion of mass and heat at the interface between the laser and saturable absorber gas flows. The results show that the growth of the mixing zone is linear, $\alpha = 0.1$, and the spreading of heat and mass are mutually equal. The interferometric data show that for CO_2 wavelength radiation (10.6 μ) the turbulent mixing at the interface has little effect on the optical quality of the porous tube-generated flowfield for differences in β up to about 15%.

I. Introduction

A MAJOR element in the laser fusion program is the availability of scalable nanosecond carbon dioxide laser amplifiers. One of the key technical questions for device scaling and for maximum performance is the development of scalable gain isolation. Flowing a saturable absorber gas together with the laser gas in the cavity is a novel scheme to provide windowless gain isolation. In order to optimize the operation in such a cavity, the diffusion of the saturable absorber into the laser gas is of significant importance.

In this type of device, to optimize performance it also becomes desirable to flow the gas parallel to the electric field (Fig. 1). To achieve the latter, we use a recently developed scheme[1] that is based on generating a flowfield in a cavity by injecting gas through a grid of porous tubes. Figure 2 indicates the flow geometry for the main flow and saturable absorber flow.

The present work deals with results of investigations concerning the distribution of velocity, temperature, and species concentration at the interface between two flowfields generated by two adjacent grids of porous tubes, and the degradation of the optical quality of the flow by the turbulent mixing that takes place in this zone. Measurements have been carried out in a cavity where one portion of the flow was thermally tagged or mixed with a tracer gas, with the initial differences in temperature and concentration with respect to the surrounding flow confined to small values.

II. Experimental Apparatus

A schematic of the apparatus that has been constructed and used for our experiments is shown in Fig. 3. The porous tubes used here are manufactured by Mott Metallurgical, Farmington, Conn. The tubes are fabricated from metallic powder (S.S. 316) to yield tubes with controlled porosity. The powder is precompressed into a form by the application of a controlled pressure, and subsequently heated to the sintering temperature. The tubes used here were eccentric in their cross section with a 0.10 cm thin wall, 0.63 cm i.d., 0.95 cm o.d. and 33 cm long. A detailed description of the eccentric tubes characteristics is given by Tong et al.[2]

Because of the longitudinal pressure drop inside the porous tube induced by the axial flow, the radial pressure drop through the tube wall itself was designed to be large in order

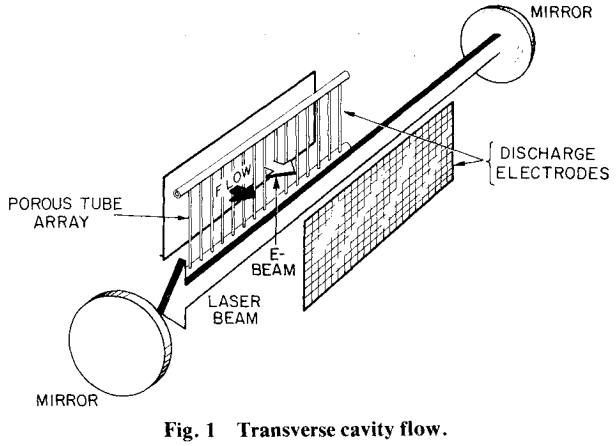

Fig. 1 Transverse cavity flow.

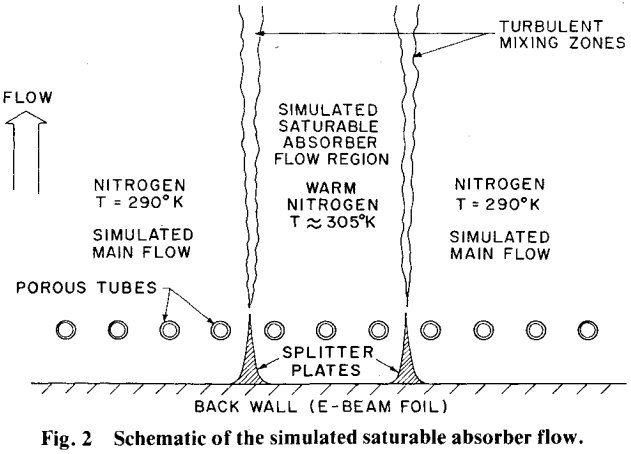

Fig. 2 Schematic of the simulated saturable absorber flow.

Presented as Paper 78-178 at the AIAA 16th Aerospace Sciences Meeting, Huntsville, Ala., Jan. 16-18, 1978; submitted Dec. 26, 1978; revision received July 9, 1979.

Index categories: Experimental Methods of Diagnostics; Jets, Wakes, and Viscid-Inviscid Flow Interactions.

*Principal Research Scientist; presently with Soreq Nuclear Research Center, Yavne, Israel. Member AIAA.

†Senior Research Scientist; presently with Arthur D. Little, Cambridge, Mass. Member AIAA.

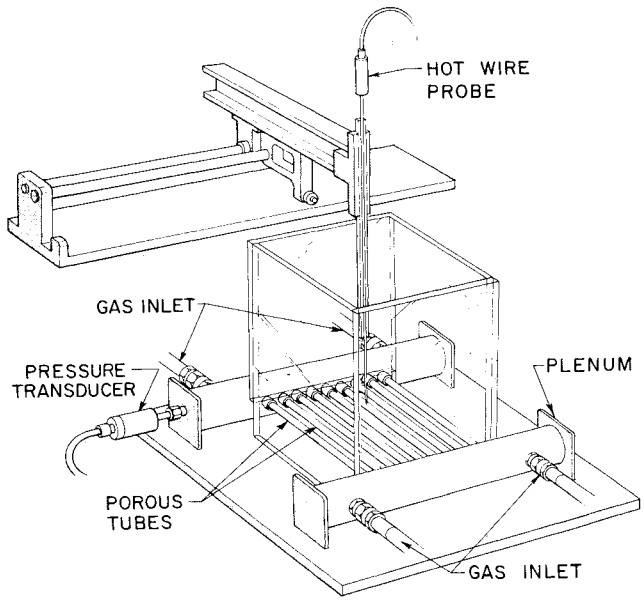

Fig. 3 Experimental setup.

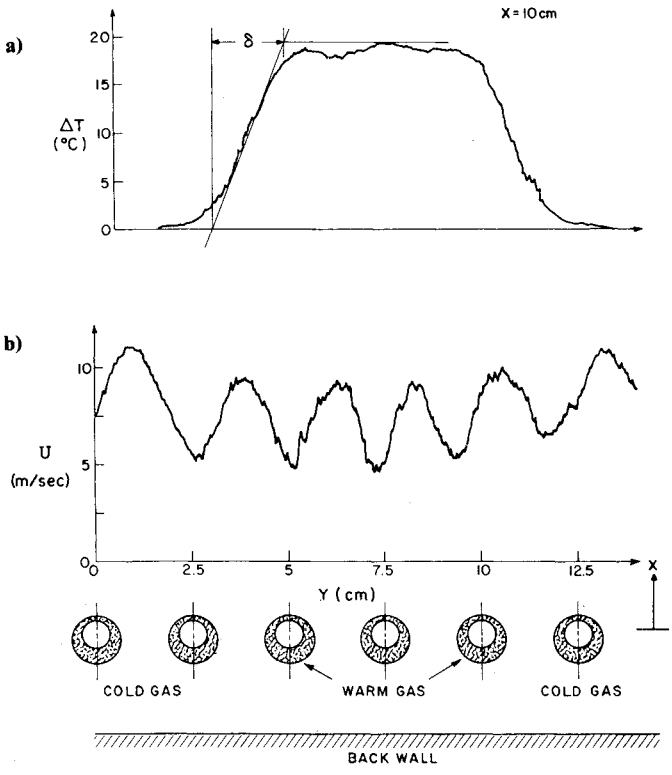

Fig. 4 Temperature distribution and velocity flowfield 10 cm downstream of the porous tube array.

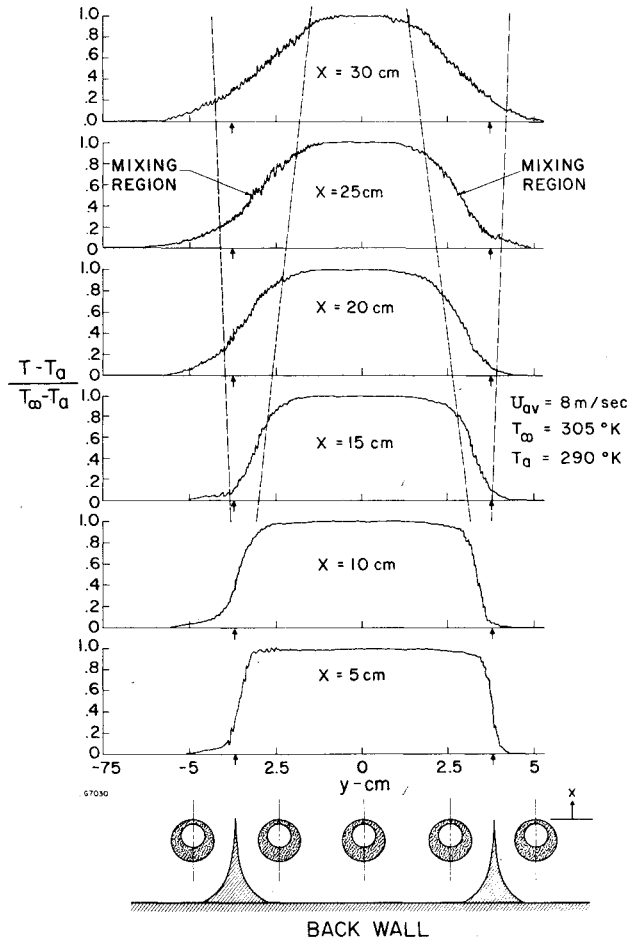

Fig. 5 Spatial development of temperature diffusion in the porous grid generated flow.

that the radial mass injection rate be uniform along the tube length. To insure the latter, very low porosity tubes were used here, designated by the manufacturer as having 0.5 μ filtration rating.

The porous tubes were arranged in a parallel grid and connected to two large diameter pipes (5.0 cm i.d.). The tubes were fed from two high-pressure nitrogen manifolds, one serving as a flow source plenum for the room temperature nitrogen and the other for the slightly heated nitrogen. The parallel porous tube array (28 cm × 33 cm in overall dimensions) was enclosed in a 30-cm-high plexiglass enclosure to prevent entrainment of ambient air into the near-field of the porous tube-generated flow.

Compressed nitrogen was supplied to the grid from a high-pressure bottle bank. The supply pressure was regulated using a dome pressure regulator which ensured constant plenum pressure during each test run. No filtration of the gas was used and no degradation of the low-porosity tube flow capability was observed over a large number of tests.

III. Flowfield Structure

Hot wire anemometry was used for mean flow velocity and rms velocity fluctuation measurements. The constant temperature hot wire system (Thermo-Systems, Inc.) consisted of a constant temperature anemometer in conjunction with a linearizer yielding a linear net calibration curve. A true rms voltmeter served to obtain rms velocity fluctuations, and (in conjunction with an analog divider) yielded turbulence intensity data.

A typical hot wire measurement of the velocity flowfield 10 cm downstream of the porous tube array is shown in Fig. 4b. The porous tubes were spaced at a distance $2c = 2.5$ cm apart and 2.5 cm from the back wall. Holding the plenum pressure constant at $p_0 = 200$ psig, the mean axial velocity distribution and the turbulent velocity fluctuations were measured at several downstream sections. In general, the flow displayed a wake-like behavior[1,2] with small variations present between the different wakes, presumably due to some nonuniformities in the injection through the different porous tubes. The large velocity nonuniformities associated with the wake-like flow rapidly decayed, and at about $x/2c \sim 10$ the mean flow became quite uniform. Similar velocity measurements at higher plenum pressures were made by Tong et al.[2] A detailed evolution of the velocity flowfield downstream of the porous tube array is displayed in this reference.

IV. Temperature Measurements

We have investigated the structure of the temperature field in the interface between the simulated laser gas flow and the saturable absorber flow. For this purpose the "saturable absorber" gas was heated slightly ($\Delta T \approx 15°C$) utilizing a pebble bed as a heat exchanger. The gas, nitrogen in our case, was preheated by flowing through the pebble bed and was then introduced into the three porous tubes that generated the "saturable absorber" flow region (Fig. 2). These tubes were equipped with thermocouples, glued to the surface at various axial positions, which served to monitor the heated gas temperature during each test to insure that data were taken under temporally stable heating conditions. The splitter plates shown in Fig. 2 were used in an attempt to reduce the growth of the turbulent mixing layers.

For measuring mean temperature distributions, both very fine thermocouples (wire size 0.0005 in.) and a constant current hot wire anemometer, operating as resistant thermometer, were used. The hot wire was also used to measure temperature fluctuations, and in conjunction with a true rms voltmeter (TSI), yielded rms temperature fluctuation data. A typical expanded profile of the temperature distribution in the mixing zone and the corresponding velocity distribution is shown in Fig. 4a. This figure also includes the definition of the mixing zone width.

Figure 5 displays the evolution of the temperature distribution across the mixing layers with downstream distance. The initial distribution is effectively rectangular—which is quite remarkable considering the nonuniform structure of the velocity field at this location. As one proceeds downstream, the spreading into the ambient surroundings becomes evident. The rate of the spreading of the temperature field is shown in Fig. 6. In this figure we present data of the mixing layer growth taken with and without the presence of the splitter plate. Interestingly, the initial mixing layer is smaller when the splitter plate is used; however, the mixing layer rate of growth is about the same as without the splitter plate further downstream of the porous tube grid. This is because, beyond about 10 cm from the porous tubes, the turbulent flowfield is not affected by the presence of the splitter plate.

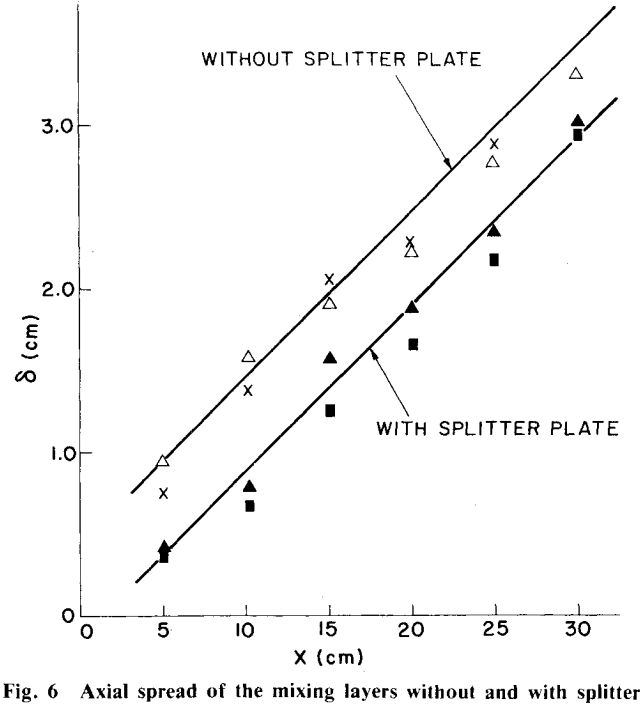

Fig. 6 Axial spread of the mixing layers without and with splitter plates between the warm gas-cold gas tube arrays. Plenum pressure 100 psi (△ , ▲) and 200 psi (X, ,).

V. Species Concentration Measurements

Mass diffusion in the turbulent mixing layers between the laser gas and saturable absorber flow was measured using an infrared (IR) absorption technique. The scheme involved seeding the saturable absorber region with SF_6, which was used as a tracer in the mixing region. A small gas extraction probe sampled various locations in the mixing layers. The concentration of SF_6 was then determined from the absorption of radiation from a low-power CO_2 laser beam.

A schematic of the experimental setup for the absorption measurement is shown in Fig. 7. The laser beam from a low-power (4 W) GTE-Sylvania 941E CO_2 laser was chopped at a frequency of 1000 Hz and attenuated to about half its power before it entered a 50% beam splitter generating the reference beam and the beam that goes through the absorption bell. The intensities of the reference beam I_0 and the transmitted beam I_t were recorded by two pyroelectric detectors (Molectron P003). A balance amplifier (not shown) was used for the transmitted beam to insure that the detector outputs are equalized before introduction of SF_6 into the cell. In Fig. 7 we show an alternate way of equalizing the detector outputs before introduction of SF_6 by using an adjustable attenuator for the reference beam.

When absorbing gas flows into the cell, the transmitted CO_2 radiation is:

$$I_t = I_0 e^{-\alpha P x} \tag{1}$$

where α is the absorption coefficient, P is the partial pressure of the absorbing gas (SF_6), and x is the absorption cell length.

The absorption coefficient α depends strongly on the wavelength of the laser radiation. In order to insure that a measurement has been made at a stable laser wavelength, a small fraction of the laser radiation was recorded by a spectrum analyzer. The two most stable laser wavelengths were at 10.59 and 10.57 μ.

In the test section shown in Fig. 7 half of the porous tubes were fed with pure N_2 and the rest with N_2 where SF_6 was mixed at concentrations of about 5×10^{-4} to 3×10^{-3}. A gas extraction probe sampled the mixing layers at several elevations from 3 to 30 cm above the porous tubes and scanned continuously the mixing layers with the aid of a traversing mechanism. The total "run time" was 25 s. During this time interval the probe scanned 4 cm in the mixing layer.

Figure 8 shows the species concentration probe. The probe was made of plexiglass and consisted of two parts. A screen was inserted between the two parts to insure that the diverging flow of the sampled gas fills the test section of the probe. Two 1-in.-diam optical quality germanium windows were inserted in the test section of the cell to allow the transmission of the CO_2 laser radiation through the cell. The absorption cell length x was 0.64 cm. The sampled gas flowing through the probe was sucked with a 1-mm-diam, 10-cm-long hypodermic tube.

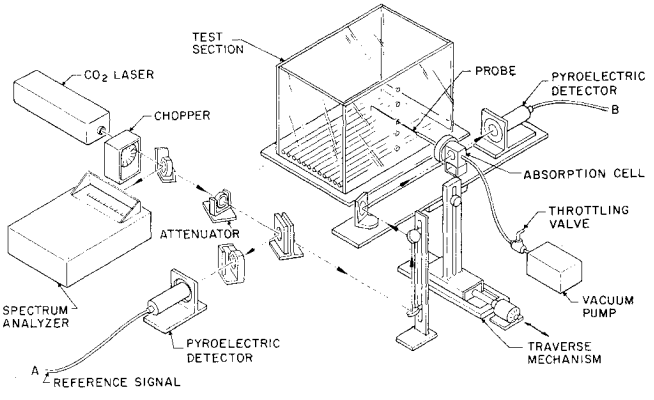

Fig. 7 Schematic of the species concentration IR absorption measurement.

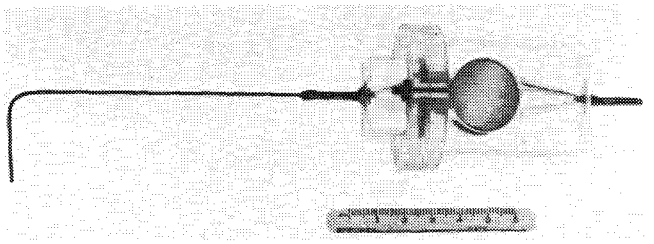

Fig. 8 The species concentration probe.

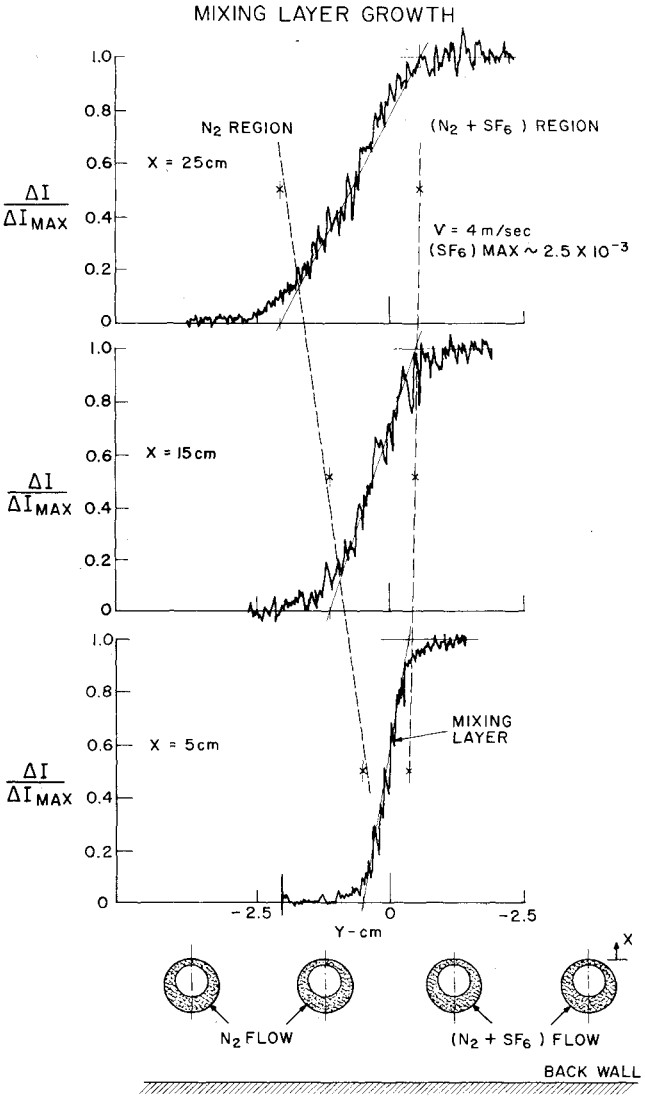

Fig. 9 Spatial development of species concentration diffusion in the porous grid generated flow.

The spatial resolution of the probe was equal to the sampling tube size which was picked, equal to 1 mm. This corresponds to a resolution of 3-10% of the mixing layer thickness. The relatively large size of the sampling tube was selected to minimize the response time of the probe and enable continuous measurements in the mixing layers rather than pointwise measurements.

The response time of the probe was

$$\tau = \frac{\ell_1}{u_1} + \frac{\ell_2}{u_2} = 0.18\,\text{s} \qquad (2)$$

where the length of the sampling tube $\ell_1 = 10$ cm, the length of the cell $\ell_2 = 4$ cm, the sampling velocity for isokinetic suction,

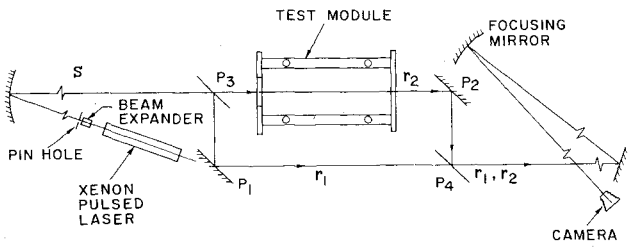

Fig. 10a The Mach-Zehnder interferometer.

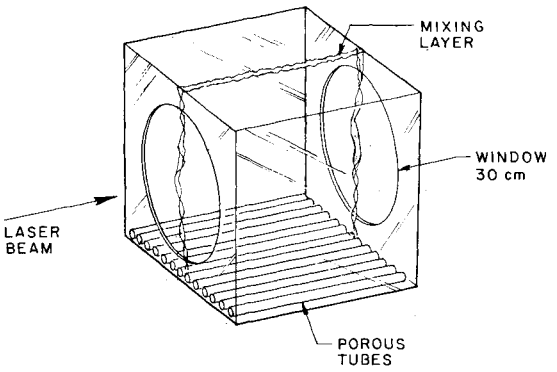

Fig. 10b Optical setup in rectilinear test section.

$u_1 = 5$ m/s, and the velocity through the cell $u_2 = u_1 x$ (area of tube/area of cell) $= 0.05\,u_1$.

The SF_6 concentration resolution was equal to about 2×10^{-4}. This can be determined from Eq. (1). Using $\alpha \simeq 0.4$ Torr^{-1} cm^{-1}, $x = 0.64$ cm, and $P = 760\,(2 \times 10^{-4})$ Torr, the relative absorbed radiation is about 4% and can easily be detected.

In our results shown in Fig. 9, the concentration C_{max} of SF_6 in the simulated saturable absorber region was equal to about 2.5×10^{-3} by volume. The relatively high concentration of SF_6 was picked in order to have an acceptable signal to noise ratio in the low SF_6 concentration region of the mixing layer. In the high SF_6 concentration region of the mixing layer, the problem was then that the IR absorption profile was not proportional to the SF_6 concentration profile of the mixing layer since Eq. (1) is not linear at high SF_6 concentrations. Nevertheless, in determing the thickness of the mixing layer from the IR absorption profile rather than the corresponding SF_6 concentration profile, we found that the error was less than 1%.[3] In view of the fact that the overall error of the IR absorption method due to spatial resolution and time response was of the order of 5%, the present error was neglected. The IR absorption profiles were used directly and were not corrected to give the true concentration distribution profiles in the mixing layers. Figure 9 illustrates the spreading of the mixing layer as obtained by the species concentration probe. These results are almost identical to the data of temperature diffusion obtained under the same flow conditions and are presented in Figs. 5 and 6. This result is to be expected here since under the present flow conditions there is a complete analogy between the transports of heat and mass.[4,5]

VI. Interferometric Visualization of Heat and Mass Diffusion

Heat or mass diffusion in the mixing layers between the simulated laser gas and saturable absorber gas flows was also studied and visualized with the use of a Mach-Zehnder interferometer.[6] Figure 10a shows a schematic of the interferometric set up. The system consisted of 30-cm-diam optical elements which were mounted on a vibration isolation table to ensure mechanical stability. A pulsed xenon laser

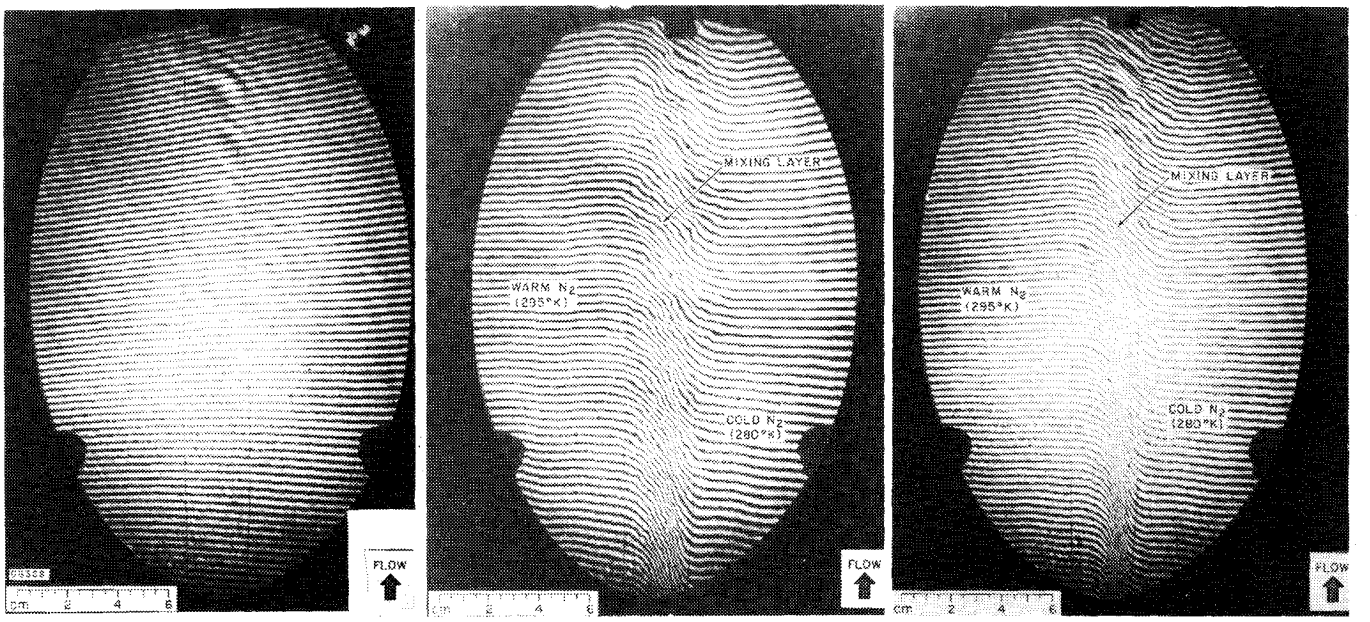

Fig. 11 a) No-flow interferogram. b) Interferogram of the mixing layer between the two gas streams of Fig. 10b with a temperature difference $\Delta T = 10°C$. Vertical wires 2.5 cm apart, horizontal wire 18 cm above the porous tubes. c) Same as Fig. 11b with the addition of a splitter plate between the tubes at the mixing region.

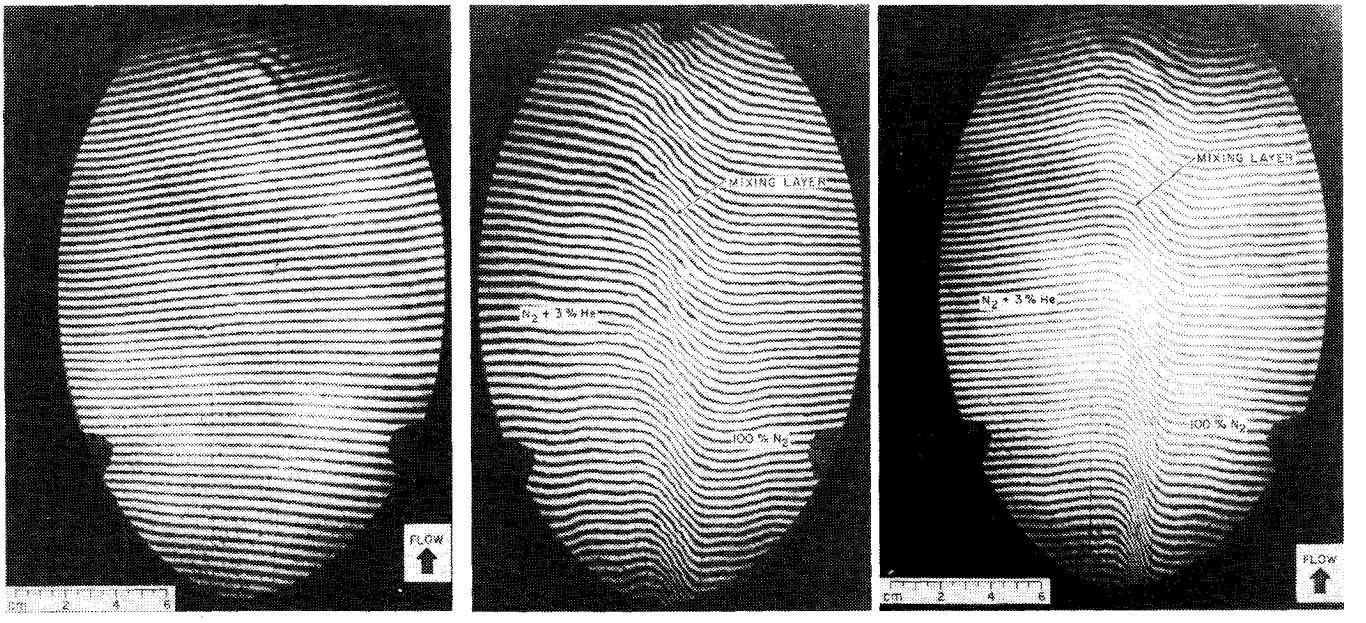

Fig. 12 a) No-flow interferogram. b) Interferogram as in Fig. 11b with helium addition into one of the streams. Vertical wires 2.5 cm apart, horizontal wire 18 cm above the porous tubes. Helium concentration 3% by volume. c) Same as Fig. 12b with the addition of a splitter plate between the tubes at the mixing region.

radiating at 5127 Å with a pulse length of 0.3 μ s was used as the illumination source. The laser beam was expanded using a 40:1 beam expander to fill the 30-cm-diam optical elements.

The Mach-Zehnder interferometer was used in the rectilinear test section with the porous tubes parallel to the optical beam axis as shown in Fig. 10b. Half of the tubes were fed with room temperature nitrogen ($T \sim 280$ K) and the rest of the tubes with lower density gas which was either nitrogen slightly heated ($T \sim 295$ K) or nitrogen with a small concentration of helium (about 3% of volume).

Direct visualization of the mixing layers between the two gas streams was achieved with this arrangement and some typical interferograms are shown in the following figures. Figure 11a is a tare shot (an interferogram without flow in the test section) with the fringes almost horizontal. Figure 11b shows a typical interferogram of the mixing layer between the two gas streams with a small temperature difference.

One notices the mixing layer region and the characteristics of its spreading. The fringe shift in the mixing region is proportional to the density difference, which in turn is proportional to the temperature difference from the reference stream (i.e., the cold nitrogen stream on the right of the photograph). Close to the tubes, in the lower part of the photograph, the mixing layer thickness is small and steep temperature gradients are apparent. The gradients diffuse, that is, the mixing layer grows as the gases move upward. The two vertical wires in the photograph are 2.5 cm apart and the horizontal wire is 18 cm above the porous tubes. The mixing

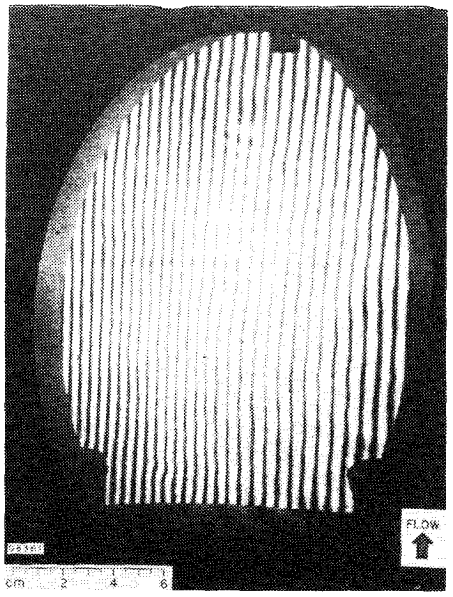

Fig. 13a No-flow interferogram.

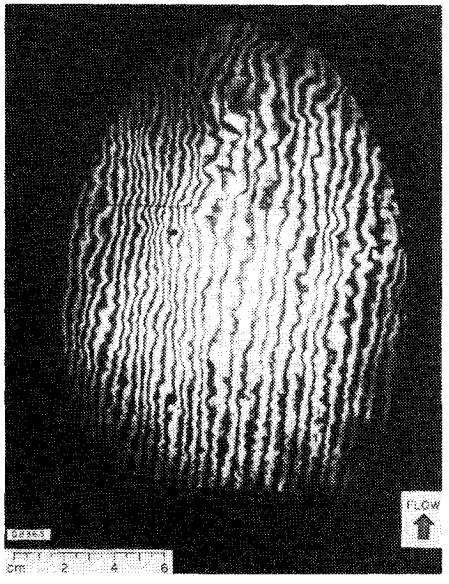

Fig. 13b Interferogram of porous tube flow with 9% index of refraction variation between the parallel gas streams of Fig. 2. Vertical wires 1.3 cm apart, horizontal wire 18 cm above the porous tubes.

layer thickness grows to about 2.5 cm at a distance of 25 cm above the porous tubes, and this result is consistent with the hot wire temperature measurements presented in Fig. 6.

Figure 11c shows a similar interferogram of heat diffusion. In this case a splitter plate was inserted between the porous tubes at the mixing region, and the thickness of the mixing region near the tubes at the lower part of the photograph is smaller than it was in Fig. 11b. The growth characteristics of the mixing layer are as in Fig. 11b.

Figures 12a-c are similar to Figs. 11a-c and show the mass diffusion characteristics between the gas streams. In this case the lower density gas was nitrogen with a small concentration of helium (about 3% by volume). The interferograms without a splitter plate (Fig. 12b) and with a splitter plate (Fig. 12c) exhibit the same behavior as the heat diffusion interferograms of Figs. 11b and 11c.

An analytic investigation of heat or mass diffusion in the present flowfield has been undertaken in Ref. 3. The analysis is an extension of a vorticity transport model used in Ref. 1 with the addition of a scalar (heat or mass) diffusion

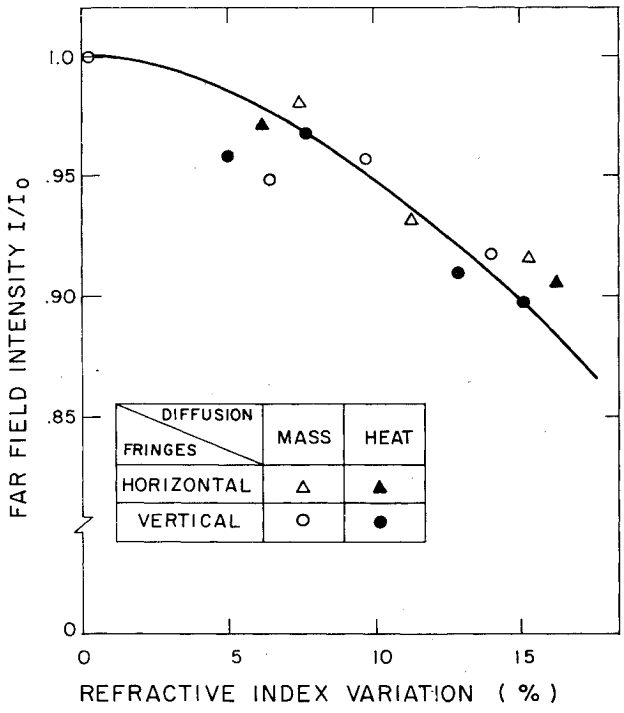

Fig. 14 Optical beam intensity attenuation at 10.6 μ caused by two turbulent mixing layers.

equation. The results, assuming constant turbulent Schmidt or Prandtl numbers equal to 1.0 and a turbulent Reynolds number $Re_t = 17.0$ (consistent with Ref. 2), deviate slightly from the experimental measurements.

VII. Optical Medium Homogeneity

The optical medium homogeneity in the laser cavity and the beam degradation caused by the mixing layers between the laser gas and saturable absorber gas flows was next investigated. The basic instrument for this investigation was a Mach-Zehnder interferometer with 30-cm-diam optical elements described above. The laser beam axis was perpendicular to the porous tubes with the flowing gases of different refractive indices forming two mixing layers as in Fig. 2. Both cases of heat diffusion, simulating the saturable absorber gas diffusion into the laser gas and actual mass diffusion, were investigated. Single short exposure (0.3 μs) interferograms were taken in the test section covering index differences between the flowing gases from 5-15%. Typical interferograms are shown in Figs. 13a and 13b. Figure 13a is a no flow reference interferogram and Fig. 13b is a flow interferogram with 9% index variation between the two gases. Notice in Fig. 13b the wiggles introduced into the fringe pattern by the turbulent mixing of the two gases having different indices of refraction. From this and other similar interferograms the expected far-field intensity I/I_0 has been obtained using the procedure outlined in Ref. 3.

The primary effect of the turbulence in the mixing layers is fluctuations of the gas density which cause fluctuations in the index of refraction, since

$$n = 1 + (n_0 - 1)(\rho/\rho_0) = n_0 + \Delta n' \tag{3}$$

(Ref. 6), where

$$\Delta n' = (n_0 - 1)(\Delta\rho/\rho_0) \tag{4}$$

and the subscript 0 refers to average conditions.

Beam degradation is mainly caused by phase distortion which can be estimated from Ref. 7.

$$\Delta\psi' \approx \sqrt{2}\frac{2\pi}{\lambda}\sqrt{\overline{\Delta n'^2}}\sqrt{\Delta L} \tag{5}$$

where λ is the wavelength of the incident light, $\sqrt{\Delta n'^2}$ is the rms fluctuation of the refractive index in the mixing layer, which is proportional to the difference of the refractive indices of the two flowing gases, Λ is the integral length scale of turbulence, and L is the thickness of the mixing layer. The far field intensity I is then[6]

$$I/I_0 = \exp(-\Delta\psi'^2) \simeq 1 - \Delta\psi'^2 \tag{6}$$

where I_0 is the intensity of the incident beam.

The results for the far-field intensity attenuation of the optical beam caused by two mixing layers for the cases of heat or mass diffusion in the test section of Fig. 3 are presented in Fig. 14 as a function of the refractive index variation of the flowing gas streams. The solid line in Fig. 14 is a best-fit curve through the experimental data such that the intensity attenuation is proportional to the square of the refractive index variation according to the theoretical predictions of Eqs. (5) and (6). The results show that the effect of the two mixing layers between the gas streams on a CO_2 laser beam is about a 10% attenuation of the beam intensity for a 15% difference in the index of refraction of the two gases.

VIII. Conclusions

Based on the experimental results presented, the following conclusions can be drawn regarding the diffusion of heat or mass in a porous tube generated flowfield.

1) The rates of spreading of heat or mass in the flowfield generated by an array of eccentric porous tubes are mutually equal. A linear growth of the mixing layer with downstream distance, equal to 0.10 x, was measured. This result was obtained by all experimental methods used.

2) A novel species concentration probe based on IR absorption has been developed in the present study and utilized in the species concentration measurements.

3) Optical medium homogeneity measurements have shown that a 10% attenuation in CO_2 laser beam intensity should be expected from two turbulent mixing layers, for 15% difference in index of refraction between adjacent flowing gas streams generated by parallel arrays of porous tubes.

Acknowledgment

This work was supported under ERDA Contract EY-76-C.

References

[1] Avidor, J. M., Kemp, N. H., and Knight, C. J., "Experimental and Theoretical Investigation of Flow Generated by an Array of Porous Tubes," *AIAA Journal*, Vol. 14, Nov. 1976, pp. 1534-1540.

[2] Tong, K. O., Knight, C. J., and Avidor, J. M., "Flow Generated by an Array of Eccentric Porous Tubes," AIAA Paper 77-662, Albuquerque, N. Mex., June 1977.

[3] "Scalable Nanosecond Laser Technology," section on Flowing Saturable Absorber, Final Report, prepared for United States Department of Energy, Contract No. EY-76-C-02-4055, AERL, Dec. 1977.

[4] Launder, B. E., "Heat and Mass Transport," *Topics in Applied Physics Vol. 12—Turbulence*, edited by P. Bradshaw, Springer-Verlag, New York, 1976, pp. 231-287.

[5] Hinze, J. O. and Van Der Hegge Zijnen, B. B., "Transfer of Heat and Matter in the Turbulent Mixing Zone of an Axially Symmetric Jet," *Applied Science Research*, Vol. A1, 1949.

[6] Born, M. and Wolf, E., *Principles of Optics*, Pergamon Press, New York, 1964.

[7] Sutton, G. W., "Effect of Turbulent Fluctuations in an Optically Active Fluid Medium," *AIAA Journal*, Vol. 7, Sept. 1969, pp. 1737-1743.